Ocean Engineering 259 (2022) 112088

Contents lists available at ScienceDirect

Ocean Engineering

journal homepage: www.elsevier.com/locate/oceaneng

Vibration suppression of multi-component floating structures via passive TMDs and Bayesian ascent

Xiantao Zhang [a], Da Lu [a], Hongyang Dong [b], Xiaowei Zhao [b,*], Feargal Brennan [c], Yibo Liang [c]

[a] State Key Laboratory of Ocean Engineering, Shanghai Jiao Tong University, Shanghai, China
[b] Intelligent Control & Smart Energy (ICSE) Research Group, School of Engineering, University of Warwick, Coventry, UK
[c] Offshore Engineering Institute, University of Strathclyde, Glasgow, UK

ARTICLE INFO

Keywords:
Multi-component floating structure
Hydrodynamics
Vibration suppression
Tuned mass damper
Bayesian ascent

ABSTRACT

This paper aims to achieve vibration suppression for multi-component floating structures under ocean waves. To this end, a multiple-passive-TMD (tuned mass damper) structure is employed, and a numerical model is developed incorporating both the dynamics of a hinged floating foundation and passive TMDs. A data-driven parameter optimization method is developed to search for optimal TMD parameters. This method is built upon Bayesian Ascent (BA) – an advanced sequential searching strategy for optimizing black-box functions, combining the merits of both the Bayesian Optimization method and the gradient-free trust-region algorithm. Simulation results under different wave conditions verify the effectiveness of the BA-based parameter selection method, showing that the resulting passive TMDs can significantly reduce the vibration of the whole floating structure.

1. Introduction

Floating foundations are widely used in offshore regions for various purposes, such as oil and gas exploration, offshore wind platforms, ocean observation and monitoring, etc. Due to offshore floating foundations are often located in ocean regions with harsh environmental conditions over long time periods, they are inevitably subjected to different types of environmental loads, including wave, wind, and current (Faltinsen, 1993). These environmental loads may cause vibrations or motions of offshore foundations, which may pose significant negative effects, such as fatigue failure of structures, degraded efficiency in operations, and discomfort of crews. Therefore, it is always of great significance to find out proper ways to mitigate the structural loads and motions of offshore floating foundations.

There have been a lot of researches focusing on vibration/motion reduction control of single offshore foundations (and the foundations themselves are commonly regarded as rigid structures) (Zhang et al., 2017), such as viscoelastic mechanisms (Patil and Jangid, 2005), damping isolation mechanisms (Ou et al., 2007), and dynamic vibration absorbers. One popular example of dynamic vibration absorbers is the tuned mass damper (TMD) (Hoang et al., 2008; Alexander and Schilder, 2009). A typical TMD module usually consists of a mass, a spring and a damper. By properly setting the parameters of spring & damper and/or providing additional external forces, TMD is expected to act as a "counteragent" and absorb the kinetic energy that induces the main plant's vibration, reducing the whole structure's maximum vibration amplitude while weighing much less than it (a TMD module usually weights 2%–6% of the whole plant Kundu, 2012; Stewart and Lackner, 2013; Lackner and Rotea, 2011; Fitzgerald et al., 2018; Li and Gao, 2015; Zhang et al., 2020; Park et al., 2019). TMDs have been widely used to suppress the vibrations of large structures, such as skyscrapers (Zhou et al., 2022) and bridges (Xu et al., 2019; Yin et al., 2019). In general, TMDs can be categorized into three main types: passive TMD (Stewart and Lackner, 2013; Lackner and Rotea, 2011), active TMD (Fitzgerald et al., 2018; Li and Gao, 2015; Zhang et al., 2020), and semi-active TMD (Park et al., 2019). Passive TMD has constant spring stiffness and damping coefficient. In contrast, active TMD employs actively powered actuators to generate an extra control force, aiming to achieve enhanced control performance. But active TMD has critical drawbacks, including high power consumption and stability issues. Semi-active TMD provides additional control freedoms by modifying the parameters of TMDs (damping coefficient and spring stiffness) instead of directly applying additional forces to the TMD. But semi-active TMD still needs external power sources, and it is typically hard to build. Due to these facts, the passive-stability and low-cost features of passive TMD render it currently the most popular type among the three options in practical applications.

* Corresponding author.
E-mail addresses: zhxt@sjtu.edu.cn (X. Zhang), nichenrugu@sjtu.edu.cn (D. Lu), hongyang.dong@warwick.ac.uk (H. Dong), xiaowei.zhao@warwick.ac.uk (X. Zhao), feargal.brennan@strath.ac.uk (F. Brennan), yibo.liang@strath.ac.uk (Y. Liang).

https://doi.org/10.1016/j.oceaneng.2022.112088
Received 4 April 2022; Received in revised form 15 June 2022; Accepted 19 July 2022
Available online 2 August 2022

TMDs are suitable and widely-employed choices for the vibration/motion suppression of floating structures. A prototypical application scenario of TMDs in ocean engineering is related to offshore wind foundations' vibration/motion suppression control. The motions of a floating platform can have negative effects on the whole platform's structural integrity and the wind turbine's power capture efficiency (Wen et al., 2018). Yang et al. (2019) applied a passive TMD in a barge-type offshore wind floating foundation and derived its parameters by the frequency tuning method and generic algorithm. Yang and He (2020) investigated the vibration suppression effect of a two-TMDs mechanism (one in the platform and the other in the turbine's nacelle) for a spar-type offshore wind turbine, showing that TMDs can successfully mitigate the structural vibration of offshore floating wind turbines. The effectiveness of TMDs in the motion/vibration suppression of TLP-type offshore wind floating foundations was explored and proved by Wu and Li (2020). Li and Gao (2015) proposed a robust control method to suppress a floating turbine's vibration via an active TMD. Based on the same simulator as in Li and Gao (2015) and Zhang et al. (2020) designed a reinforcement learning algorithm to control TMD. In addition, TMD-based motion/vibration suppression methods also have been applied to many other types of floating structures. For example, based on numerical simulations, Jin et al. (2021) found that the hydro-elastic transient motion and mooring tensions of a submerged floating tunnel under seismic excitation were significantly reduced by using an optimized TMD.

Apart from single offshore floating platforms/foundations, interconnected multi-component floating structures are also widely employed in various engineering scenarios, such as hinged wave energy converters (Yu et al., 2016), multi-component very large floating structures used as airports (Zhang et al., 2018), etc. Zhang et al. (2021) proposed a "one-platform-multi-turbines" concept using a hinged multi-component floating structure as the floating foundation. Except for wave energy converters whose motions are expected to be enlarged for improving power efficiency, most interconnected floating structures expect to mitigate their vibration/motion to ensure structural integrity (such as for very large floating structures) and/or power capture efficiency (such as for offshore wind turbines). Some researchers applied wave energy absorption units at the interconnection to suppress the motion of the multi-component floating structure and capture energy in the meantime (Zhang et al., 2019a,b). Although the TMD's effectiveness in the vibration/motion suppression of single floating platforms has been widely studied, there lacks direct evidence of their effectiveness in multi-component floating structures. It is noteworthy that the dynamical interactions and movement couplings of different components in a large floating structure make the selection of TMD parameters challenging. Conventional methods that depend on natural frequencies are no longer functional due to these inherent features associated with multi-component structures. To the authors' knowledge, it is still a research gap in developing an effective method for the design & determination of TMD structures & parameters for multi-component floating structures. We aim to fill this research gap in this paper by applying the TMD-based vibration suppression method for multi-component floating structures and designing a data-driven method to determine TMD parameters.

We employ multiple passive TMDs (every component of the whole floating structure is installed with a passive TMD) to achieve vibration/motion suppression for the whole multi-component floating structure. We note parameters (i.e. spring stiffness and damping coefficient) are the key for the employment of passive TMDs, and improper parameter choices can lead to greatly degraded vibration/motion suppression performance. Since we consider the floating structure's components are connected via hinges with each other (which is a common practice), their motions are highly coupled. This problem brings significant difficulties for the passive TMDs' parameter selection. In this paper, we propose a data-driven parameter optimization method to address this issue. Without loss of generality, a hinged three-component floating structure is taken, and a numerical model is developed incorporating both the dynamics of the hinged floating structure and passive TMDs. Based on this model, we mold the parameter optimization task of TMDs into the Bayesian Ascent (BA) algorithm (Park and Law, 2016). BA is an advanced sequential searching strategy for the optimization of black-box functions. It combines the merits of both the Bayesian Optimization (BO) method (Brochu et al., 2010) and the gradient-free trust-region algorithm (Rios and Sahinidis, 2013). One of the main advantages of BA is that a proximity constraint for the acquisition function is embedded in it, rendering the algorithm to sample states that are near to the observed optimal solutions and leading to potentially enhanced learning performance. A composite performance index considering the motions of all the components of the floating structure is employed as the reward signal, and the data from the integrated model under different TMD parameters are fed into BA to learn the optimal settings iteratively. Simulation results under different wave conditions verify the effectiveness of the BA-based parameter selection method, showing that the resulting passive TMDs can significantly reduce the vibration of the whole floating structure.

The remainder of this paper is organized as follows. Firstly the mathematical models of the hinged multi-component floating structure and TMDs are given in Section 2. The BA-based parameter optimization method for passive TMDs is proposed in Section 3. Results and discussions are given in Section 4 whereas the main conclusions are drawn in Section 5.

2. Mathematical models for floating structures and TMDs

2.1. Notations and definitions

A schematic of a hinged three-component floating structure is shown in Fig. 1. Each floater of the structure has the same dimension with length $L = 40$ m, width $B = 40$ m and height $H = 10$ m. The drift of each floater at the still water level is $D = 5$ m. We denote the global coordinate system as $\mathcal{F}_r = \{o_r, x_r, y_r, z_r\}$, where the horizontal plane $o_r x_r y_r$ coincides with the still water plane and z_r axis is positive upwards. It is noted that the distance between three floaters is set as zero in the following analysis despite that a small gap may exist between adjacent floaters in reality.

As shown in Fig. 2, for each floater/component, a body-fixed coordinate system is defined as ${}^i\mathcal{F}_b = \{{}^i o_b, {}^i x_b, {}^i y_b, {}^i z_b\}$, $i = 1, 2, 3$. Throughout the paper, the left-superscript $\cdot^r$ and $\cdot^b$ are employed to indicate that the corresponding vector is expressed in $\mathcal{F}_r$ and ${}^i\mathcal{F}_b$, respectively. In addition, we define ${}^i\boldsymbol{T}_{b/r}$ as the transformation matrix from $\mathcal{F}_r$ to ${}^i\mathcal{F}_b$ and ${}^i\boldsymbol{T}_{r/b}$ as the transformation matrix from ${}^i\mathcal{F}_b$ to $\mathcal{F}_r$. Therefore, one has ${}^i\boldsymbol{T}_{r/b} = {}^i\boldsymbol{T}_{b/r}^{\mathrm{T}} = {}^i\boldsymbol{T}_{b/r}^{-1}$. We use $S(\cdot)$ to indicate the anti-symmetric matrix of the corresponding three-dimension vector. Throughout the paper, any three-dimension vector x can be decomposed into $\boldsymbol{x} = [x_1, x_2, x_3]^{\mathrm{T}}$.

Though employing hinges can significantly reduce the floating foundation's bending moment, the downside is that this design inevitably results in larger motions than its counterpart (without hinges). As indicated in Fig. 2, we embed each floater/component with a passive TMD to suppress its pitch motion (i.e. the rotation around y_r axis). Therefore, each TMD is installed along the x_b direction of each floater. In practice, track or rail systems are usually employed to keep the movement of TMDs in the x_b direction.

2.2. Dynamics of the hinged three-component floating structure

Each floater of the hinged three-component floating structure (see Fig. 1) has six degrees of freedom and its displacement vector is defined as ${}^i\boldsymbol{\xi} = [{}^i\xi_1, {}^i\xi_2, {}^i\xi_3, {}^i\xi_4, {}^i\xi_5, {}^i\xi_6]^T$, where ${}^i\xi_j (j = 1, 2, 3)$ is the translational displacement along x_r, y_r and z_r axis, respectively, and ${}^i\xi_j (j = 4, 5, 6)$ is the rotational displacement around x_r, y_r and z_r axis, respectively. The

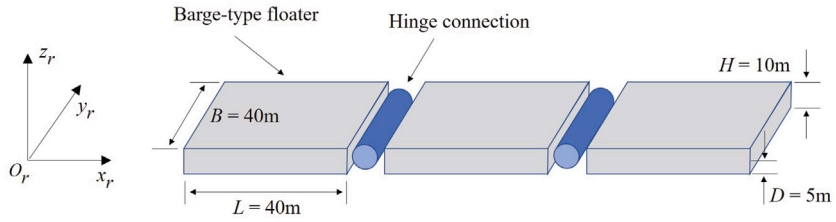

Fig. 1. A schematic of a hinged three-component floating structure.

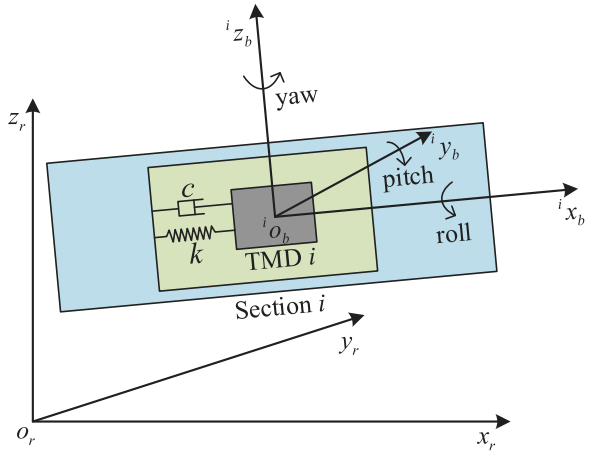

Fig. 2. Illustration of Component i with TMD i.

equations of motion for the hinged three-component floating structure are established as follows,

$$\mathbf{M}\ddot{\boldsymbol{\xi}} = \mathbf{F}_{exc}(t) - \mathbf{A}(\infty)\ddot{\boldsymbol{\xi}} - \int_{\tau=0}^{t} \boldsymbol{\Gamma}(t-\tau)\dot{\boldsymbol{\xi}}(\tau)d\tau + \mathbf{F}_h(t) + \mathbf{F}_c(t) + \mathbf{F}_{tmd}(t) \quad (1)$$

where $\boldsymbol{\xi} = [^1\xi, ^2\xi, ^3\xi]^T, \dot{\boldsymbol{\xi}}, \ddot{\boldsymbol{\xi}}$ (all with dimension of 18×1) are the displacement, velocity and acceleration vectors of the hinged floating structure, respectively; $\mathbf{M}$ is the mass matrix whose dimension is 18×18; $\mathbf{F}_{exc}$ is the wave excitation force; $\mathbf{A}(\infty)$ is the added mass matrix of the hinged floating structure at infinite frequency; $\boldsymbol{\Gamma}(t)$ is the retardation function which is related with the damping matrix $\mathbf{B}(\omega)$ as,

$$\boldsymbol{\Gamma}(t) = \frac{2}{\pi}\int_0^{\infty} \mathbf{B}(\omega)cos(\omega t)d\omega \quad (2)$$

$\mathbf{F}_h$ is the hydrostatic force; $\mathbf{F}_c$ is the force on the floating structure exerted by the hinge connection; $\mathbf{F}_{tmd}$ is the force on the floating structure exerted by the TMD implementation, the details of which are given in Section 2.3. It is noted that since no mooring system is considered (i.e. no restoring force for the motion of the floating structure in the horizontal plane), only heave, roll and pitch motions are taken into account in the following analysis. This means that the dimension of the displacement vector $\boldsymbol{\xi}$ is reduced to 9×1 and other matrices are adjusted accordingly. The force (and moment) vector for the hinge connector is denoted as $\mathbf{F}_J = \mathbf{K}_J\boldsymbol{\Psi}\boldsymbol{\xi}$, where $\mathbf{K}_J$ is the stiffness matrix used to represent the hinge connector mathematically and $\boldsymbol{\Psi}\boldsymbol{\xi}$ is the difference of the displacement at two sides of the connector with $\boldsymbol{\Psi}$ being the transformation matrix. Then the forces imposed on the centers of gravity of all floaters/components of the hinged floating structure can be described as

$$\mathbf{F}_c = -\boldsymbol{\Psi}^T\mathbf{F}_J = -\boldsymbol{\Psi}^T\mathbf{K}_J\boldsymbol{\Psi}\boldsymbol{\xi} \quad (3)$$

The specific expressions for the above-mentioned matrices such as $\mathbf{K}_J$ and $\boldsymbol{\Psi}$ are given in Appendix.

2.3. TMD embedding

In this section the dynamics of TMDs embedded in the floating structure is presented, and a novel data-driven parameter selection method for TMDs is developed via Bayesian ascent (BA) (Park and Law, 2016).

In our design, each floater/component employs a TMD to suppress its pitch angle (i.e., the rotational vibration along the y_b axis), as shown in Fig. 2. Particularly, the rotational vibration of a floater along its y_b axis will lead to the translational movement of TMD along the x_b axis. By properly setting parameters (the spring stiffness and damping coefficient), the TMD can have different moving phases from the floater, absorb and consume the kinetic energy by damping effects, and therefore suppress the whole structure's vibration. In this subsection, we deduce the dynamics of the TMD module for each floater. By combining the results in this subsection and Section 2.2, one can get the whole floating structure's dynamics.

We denote $^i\boldsymbol{r}^b_o$ as the equilibrium point of the TMD i. Without loss of generality, we assume $^i\boldsymbol{r}^b_o$ is coincident with the origin point of $^i\mathcal{F}_b$ (i.e., ^io_b). We also denote $^i\boldsymbol{r}^b_{db}$ and $^i\boldsymbol{r}^b_{dr}$ as the vector from ^io_b to TMD and the vector from o_r to TMD, respectively. In addition, $^i\boldsymbol{r}^b_{br}$ is the vector from o_r to ^io_b, and $^i\boldsymbol{\omega}^b_{br}$ is the angular velocity vector of $^i\mathcal{F}_b$ with respect to $\mathcal{F}_r$.

Based on these definitions, we have

$$^i\boldsymbol{r}^b_{db} = {}^i\boldsymbol{r}^b_{dr} - {}^i\boldsymbol{r}^b_{br} \quad (4)$$

By taking derivatives for both sides of Eq. (4) with respect to time and expressing the results in $^i\mathcal{F}_b$, one has

$$^i\dot{\boldsymbol{r}}^b_{db} = {}^i\dot{\boldsymbol{r}}^b_{dr} - {}^i\dot{\boldsymbol{r}}^b_{br} - S(^i\boldsymbol{\omega}^b_{br})\cdot {}^i\boldsymbol{r}^b_{db} \quad (5)$$

Differentiating both side of Eq. (5) again renders

$$^i\ddot{\boldsymbol{r}}^b_{db} = {}^i\ddot{\boldsymbol{r}}^b_{dr} - {}^i\ddot{\boldsymbol{r}}^b_{br} - S(^i\dot{\boldsymbol{\omega}}^b_{br})\cdot {}^i\boldsymbol{r}^b_{db} - [S(^i\boldsymbol{\omega}^b_{br})]^2\cdot {}^i\boldsymbol{r}^b_{db} - 2S(^i\boldsymbol{\omega}^b_{br})\cdot {}^i\dot{\boldsymbol{r}}^b_{db} \quad (6)$$

We denote the mass, spring stiffness and damping coefficient of TMD i by m_i, k_i and c_i, respectively. We also define the following variables: (1) $^i\boldsymbol{f}^b_g = {}^i\boldsymbol{T}_{b/r}\cdot[0,0,-mg]^{\mathrm{T}}$, which denotes the gravity vector of TMD i in $^i\mathcal{F}_b$; (2) $^i\boldsymbol{f}^b_{TMD}$, which denotes the total force applied on the mass of TMD i; (3) $^i\boldsymbol{f}^b_b = [^if^b_{b1}, {}^if^b_{b2}, {}^if^b_{b3}]^{\mathrm{T}}$, which denotes the total force applied on Component i due to the employment of TMD i; (4) $^i\boldsymbol{\tau}^b_b = [^i\tau^b_{b1}, {}^i\tau^b_{b2}, {}^i\tau^b_{b3}]^{\mathrm{T}}$, which denotes the total torque applied on Component i due to the employment of TMD i.

Then one has

$$^i\ddot{\boldsymbol{r}}^b_{dr} = {}^i\boldsymbol{f}^b_{TMD}/m_i \quad (7)$$

and here $^i\boldsymbol{f}^b_{TMD}$ follows

$$^i\boldsymbol{f}^b_{TMD} = \begin{bmatrix} -c_i\cdot {}^i\dot{\boldsymbol{r}}^b_{db1} - k_i\cdot {}^i\boldsymbol{r}^b_{db1} + {}^if^b_{g1} \\ {}^if^b_{g2} - {}^if^b_{b2} \\ {}^if^b_{g3} - {}^if^b_{b3} \end{bmatrix} \quad (8)$$

Moreover, since TMD i only moves along the ^ix_b direction, one has

$$^i\boldsymbol{r}^b_{db2} = {}^i\dot{\boldsymbol{r}}^b_{db2} = {}^i\ddot{\boldsymbol{r}}^b_{db2} = 0,\ {}^i\boldsymbol{r}^b_{db3} = {}^i\dot{\boldsymbol{r}}^b_{db3} = {}^i\ddot{\boldsymbol{r}}^b_{db3} = 0 \quad (9)$$

By summarizing all the analysis above, we can get the following results.

(1) The dynamics of TMD i along the ${}^{i}x_b$ direction:

$$
\begin{aligned}
{}^{i}\ddot{r}^{b}_{db1} = &-\frac{c_i}{m_i}\dot{r}^{b}_{db1} + [-\frac{k_i}{m_i} + ({}^{i}\omega^{b}_{br2})^2 + ({}^{i}\omega^{b}_{br3})^2]\,{}^{i}r^{b}_{db1} \\
&- {}^{i}\ddot{r}^{b}_{br1} + \frac{1}{m_i}{}^{i}f^{b}_{g1}
\end{aligned}
\tag{10}
$$

Please notice that Eq. (10) is deduced by substituting Eqs. (7)–(9) into Eq. (6) and taking the result along the ${}^{i}x_b$ direction. It should also be emphasized that there is no relative movement between TMD i and Component i along the ${}^{i}y_b$ and ${}^{i}z_b$ directions.

(2) The total additional force that is applied on Component i due to the employment of TMD i satisfies:

$$
{}^{i}\boldsymbol{f}^{b}_{b} = \begin{bmatrix} c_i\,{}^{i}\dot{r}^{b}_{db1} + k_i\,{}^{i}r^{b}_{db1} \\ {}^{i}f^{b}_{g2} - m({}^{i}\ddot{r}^{b}_{br2} + ({}^{i}\dot{\omega}^{b}_{br3} + {}^{i}\omega^{b}_{br1}\,{}^{i}\omega^{b}_{br2})\,{}^{i}r^{b}_{db1} + 2\,{}^{i}\omega^{b}_{br3}\,{}^{i}\dot{r}^{b}_{db1}) \\ {}^{i}f^{b}_{g3} - m({}^{i}\ddot{r}^{b}_{br3} - ({}^{i}\dot{\omega}^{b}_{br2} - {}^{i}\omega^{b}_{br1}\,{}^{i}\omega^{b}_{br3})\,{}^{i}r^{b}_{db1} - 2\,{}^{i}\omega^{b}_{br2}\,{}^{i}\dot{r}^{b}_{db1}) \end{bmatrix}
\tag{11}
$$

(3) The total torque that is applied on Component i due to TMD i is:

$$
{}^{i}\boldsymbol{\tau}^{b}_{b} = {}^{i}\boldsymbol{r}^{b}_{db} \times {}^{i}\boldsymbol{f}^{b}_{b} = [0,\ -{}^{i}r^{b}_{db1}\cdot{}^{i}f^{b}_{b3},\ {}^{i}r^{b}_{db1}\cdot{}^{i}f^{b}_{b2}]^{\mathrm{T}}
\tag{12}
$$

The aggregated force vector exerted on the whole floating structure by all TMDs, i.e. $\mathbf{F}_{tmd}(t)$ (see Eq. (1)), can be calculated as

$$
\mathbf{F}_{tmd}(t) = \begin{bmatrix} {}^{1}\boldsymbol{T}_{r/b}\cdot{}^{1}\boldsymbol{f}^{b}_{b} \\ {}^{1}\boldsymbol{T}_{r/b}\cdot{}^{1}\boldsymbol{\tau}^{b}_{b} \\ {}^{2}\boldsymbol{T}_{r/b}\cdot{}^{2}\boldsymbol{f}^{b}_{b} \\ {}^{2}\boldsymbol{T}_{r/b}\cdot{}^{2}\boldsymbol{\tau}^{b}_{b} \\ {}^{3}\boldsymbol{T}_{r/b}\cdot{}^{3}\boldsymbol{f}^{b}_{b} \\ {}^{3}\boldsymbol{T}_{r/b}\cdot{}^{3}\boldsymbol{\tau}^{b}_{b} \end{bmatrix}
\tag{13}
$$

By substituting Eq. (13) into Eq. (1), we are able to calculate the dynamic responses of the whole floating structure with TMDs embedding, and therefore the vibration suppression performance of the TMDs can be evaluated.

3. TMD parameter learning via Bayesian ascent

This section introduces how to decide the TMD parameters via the Bayesian ascent (BA) algorithm (Park and Law, 2016). BA is an advanced sequential searching strategy for the optimization of black-box functions. We briefly introduce the fundamental principles of BA as follows. More detailed explanations can be found in Park and Law (2016) and Brochu et al. (2010).

We denote the unknown target function to be optimized by $F : \mathcal{X} \to \mathbb{R}$, where $\mathcal{X}$ is the state domain. Without loss of generality, we consider a maximization problem, i.e., we aim to find the optimal state $\boldsymbol{x}^*$, such that

$$
\boldsymbol{x}^* = \arg\max_{\boldsymbol{x}\in\mathcal{X}} F(\boldsymbol{x})
\tag{14}
$$

As a sequential decision-making algorithm, BA selects a state $\boldsymbol{x}_n$ to observe $y_n = F(\boldsymbol{x}_n) + \epsilon$ in each learning iteration n, where ϵ is a Gaussian noise satisfying $\epsilon \sim N(0, \sigma_\epsilon^2)$. After that, BA stores (x_n, y_n) and samples the next state $\boldsymbol{x}_{n+1}$ based on all the stored data (denoted by $D^n = \{(\boldsymbol{x}_k, y_k)|k = 1, 2, \ldots, n\}$).

There are two core phases in the optimization approach: (1) *Learning/Approximation Phase*, in which an approximation strategy for $F(\boldsymbol{x})$ is needed based on the stored training data, and (2) *Optimizing/Searching Phase*, in which a sampling method for the next state $\boldsymbol{x}_{n+1}$ needs to be designed. The first phase is handled by representing $F(\boldsymbol{x})$ as a Gaussian Process (GP), formalized by

$$
p(F_{1:n}) = \mathrm{GP}(m(\cdot), k(\cdot,\cdot))
\tag{15}
$$

where $F_{1:n} = \{F(\boldsymbol{x}_1), F(\boldsymbol{x}_2), \ldots, F(\boldsymbol{x}_n)\}$, $m(\cdot)$ denotes a mean function, and $k(\cdot,\cdot)$ represents a kernel function. By optimizing the hyperparameters based on the stored training data, the posterior distribution of F can be described by the following 1-D Gaussian distribution:

$$
F \sim N(\mu(\boldsymbol{x}|D^n), \sigma^2(\boldsymbol{x}|D^n))
\tag{16}
$$

where $\mu(\boldsymbol{x}|D^n)$ and $\sigma^2(\boldsymbol{x}|D^n)$ are employed to estimate the mean and the variance of the unknown function F, respectively. They satisfy

$$
\mu(\boldsymbol{x}|D^n) = k^{\mathrm{T}}(K + \sigma_\epsilon^2\mathrm{I})^{-1} y_{1:n}
\tag{17}
$$

$$
\sigma^2(\boldsymbol{x}|D^n) = k(\boldsymbol{x},\boldsymbol{x}) - k^{\mathrm{T}}(K + \sigma_\epsilon^2\mathrm{I})^{-1} k
\tag{18}
$$

and here $y_{1:n} = \{y_1, y_2, \ldots, y_n\}$ and K denotes the kernel matrix whose (i,j)th entry satisfies $K_{ij} = k(\boldsymbol{x}_i, \boldsymbol{x}_j)$.

The optimizing/searching phase can be addressed by choosing a proper acquisition function. An example is the upper confidence bound (UCB) acquisition function, formulized by

$$
\boldsymbol{x}_{n+1} = \arg\max_{\boldsymbol{x}} [\mu(\boldsymbol{x}|D^n) + \rho^n \sigma^2(\boldsymbol{x}|D^n)]
\tag{19}
$$

where ρ^n is employed to make a trade-off between exploitation and exploration.

Another popular example is the expected improvement (EI) acquisition function, defined by

$$
\boldsymbol{x}_{n+1} = \arg\max_{\boldsymbol{x}} E[\{0, F - F^{\max}\}|D^n]
\tag{20}
$$

where $F^{\max}$ denotes the maximum target function value that is evaluated by the Learning/Approximation Phase of the nth learning iteration. After selecting the acquisition function, the next state $\boldsymbol{x}_{n+1}$ can be determined by getting its solution.

Different from BO, the BA algorithm introduces a proximity constraint for the acquisition function, such that the algorithm tends to sample $\boldsymbol{x}_{n+1}$ that is near the optimal solution observed so far (the nth iteration). To be more specific, in the Optimizing/Searching Phase, BA solves $\boldsymbol{x}_{n+1}$ by the EI acquisition function while considering a hypercube trust region, formulized by

$$
\begin{aligned}
&\boldsymbol{x}_{n+1} = \arg\max_{\boldsymbol{x}} E[\{0, F - F^{\max}\}|D^n] \\
&\text{s.t. } \boldsymbol{x} \in \boldsymbol{T} := \{\boldsymbol{x}|\|x_i - x_i^{\max}\| < \tau_i \text{ for } i = 1, 2, \ldots, p\}
\end{aligned}
\tag{21}
$$

where p is the length of $\boldsymbol{x}$; τ_i is the trust region for every entry in $\boldsymbol{x}$, and it can be adjusted during the learning process. After deciding $\boldsymbol{x}_{n+1}$ based on Eq. (21), one can observe y_{n+1} and update the training dataset. Then, the parameters in the GP approximation can be adjusted based on the updated training dataset, and $\boldsymbol{x}_{n+2}$ can be selected via the adjusted GP result. Such an iteration repeats until the state converges or meets the stopping criteria.

Based on these preliminaries, we are ready to mold our parameter selection task for multiple passive TMDs into BA. We aim to decide the spring stiffness and damping coefficient for all the TMDs. To this end, we set $\boldsymbol{x} = [\bar{k}_1, \bar{c}_1, \bar{k}_2, \bar{c}_2, \ldots, \bar{k}_h, \bar{c}_h]^{\mathrm{T}}$, where $\bar{k}_i = k_i/k_s$ and $\bar{c}_i = c_i/c_s$, and here k_s and c_s are constants that are employed for normalization purpose. We employ ${}^{i}\gamma_{\text{with\_TMD}}(t)$ and ${}^{i}\gamma_{\text{without\_TMD}}(t)$ to denote the pitch angles of Component i at time step t with and without TMD i (whose parameters are m_i, k_i, c_i), respectively. The overall performance index for the vibration suppression task is set to be

$$
F(x) = \sum_{i=1}^{h} w_i \frac{\sum_{t=0}^{T} |{}^{i}\gamma_{\text{without\_TMD}}(t)| - \sum_{t=0}^{T} |{}^{i}\gamma_{\text{with\_TMD}}(t)|}{h\sum_{t=0}^{T} |{}^{i}\gamma_{\text{without\_TMD}}(t)|}
\tag{22}
$$

where the positive constants $w_1, w_2, \ldots, w_h$ are employed for weighting purpose, h denotes the number of floaters, and T denotes the total simulation steps in one iteration. Therefore, the objective of BA is to find the optimal parameters for all TMDs (i.e., $\boldsymbol{x}^* = [\bar{k}_1^*, \bar{c}_1^*, \bar{k}_2^*, \bar{c}_2^*, \ldots, \bar{k}_h^*, \bar{c}_h^*]^{\mathrm{T}}$) subject to a pre-determined searching domain $\mathcal{X}$, such that $F(\boldsymbol{x}^*)$ can be maximized.

4. Simulation results

As discussed in Section 2, we consider a floating foundation with a size of 120 m × 40 m × 10 m, which has three floaters/components (whose size are all 40 m × 40 m × 10 m) that are connected by two hinge structures.

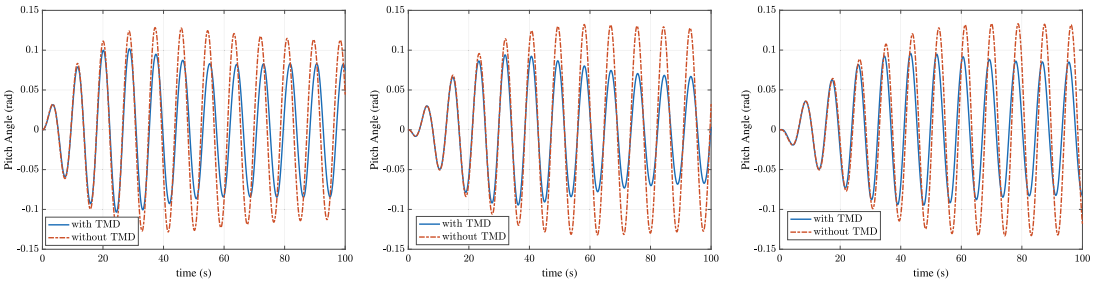

(a) Pitch angles of Component 1 (b) Pitch angles of Component 2 (c) Pitch angles of Component 3

Fig. 3. Vibration suppression results with $l = 120$ m.

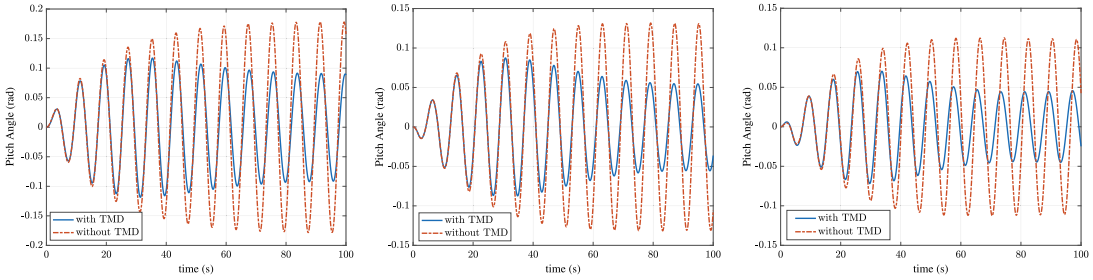

(a) Pitch angles of Component 1 (b) Pitch angles of Component 2 (c) Pitch angles of Component 3

Fig. 4. Vibration suppression results with $l = 100$ m.

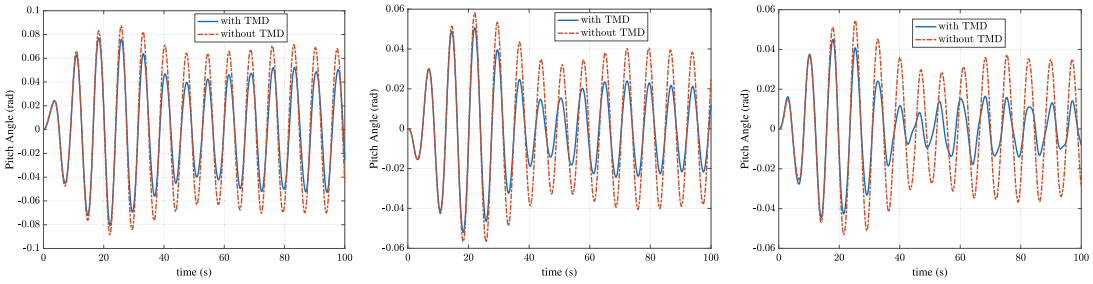

(a) Pitch angles of Component 1 (b) Pitch angles of Component 2 (c) Pitch angles of Component 3

Fig. 5. Vibration suppression results with $l = 80$ m.

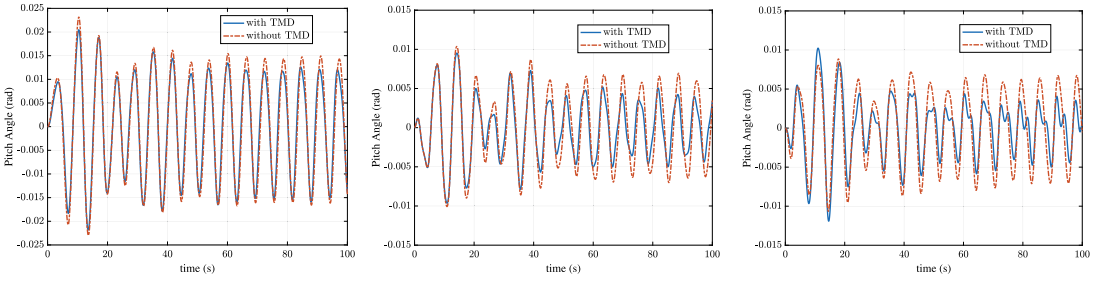

(a) Pitch angles of Component 1 (b) Pitch angles of Component 2 (c) Pitch angles of Component 3

Fig. 6. Vibration suppression results with $l = 60$ m.

The mass of each component is 8.2×10^6 kg. As we mentioned in the introduction, it is a common practice to set the TMD module to be 2%–6% of the whole structure's weight. Based on that, we set the TMD's mass to be 4% of the component's mass, i.e., $m_i = 328\,000$ kg, $i = 1, 2, 3$. Other parameters in simulations include $k_s = 107\,381$ N/m, $c_s = 8161$ N/(m/s), $T = 200$ s, and $w_i = 1$, $i = 1, 2, 3$. We employ BA to decide the spring stiffness and damping coefficient for all TMDs under four typical wavelengths: $l = 120$ m, $l = 100$ m, $l = 80$ m, and $l = 60$ m. The maximum iteration step in each testing is 200, and the searching domain is constrained by $\bar{k}_i \in (0.05, 10)$ and $\bar{c}_i \in (0.05, 10)$, $i = 1, 2, 3$.

We first test the performance of our BA-based TMD parameter optimization method under fixed wavelengths as given above. After the learning process is finished, we apply the best solutions from BA to determine TMD parameters and test their performance for each wavelength. The results are given in Figs. 3–6 and Table 1. One can see that, with the parameters tuned by BA, TMDs can significantly reduce

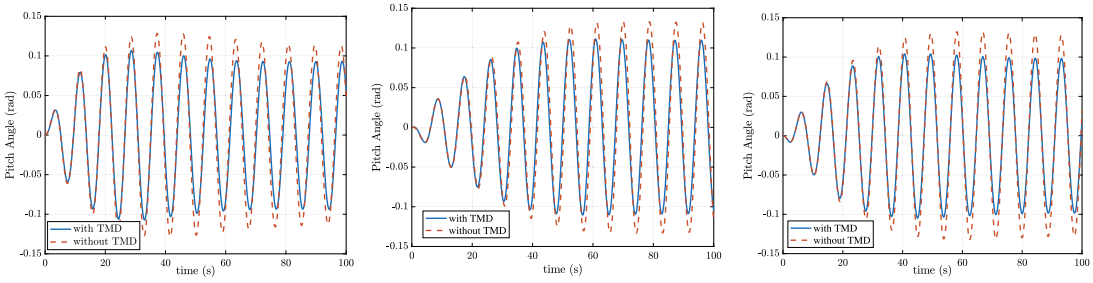

(a) Pitch angles of Component 1 (b) Pitch angles of Component 2 (c) Pitch angles of Component 3

Fig. 7. Vibration suppression results with $l = 120$ m under unified TMD parameters.

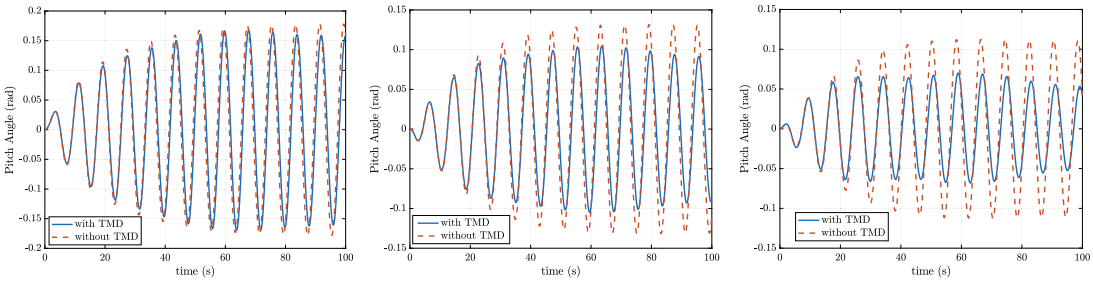

(a) Pitch angles of Component 1 (b) Pitch angles of Component 2 (c) Pitch angles of Component 3

Fig. 8. Vibration suppression results with $l = 100$ m under unified TMD parameters.

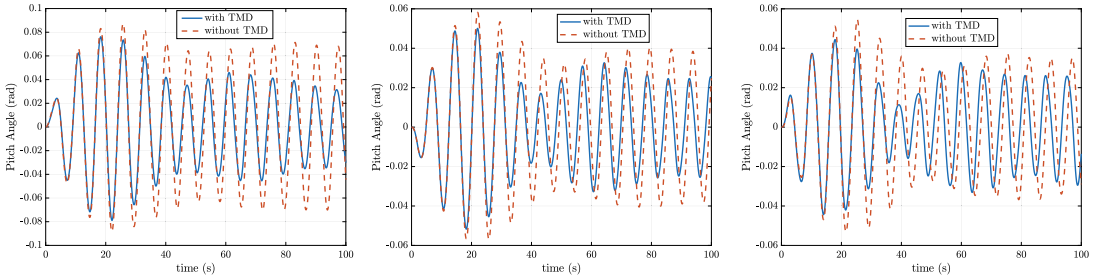

(a) Pitch angles of Component 1 (b) Pitch angles of Component 2 (c) Pitch angles of Component 3

Fig. 9. Vibration suppression results with $l = 80$ m under unified TMD parameters.

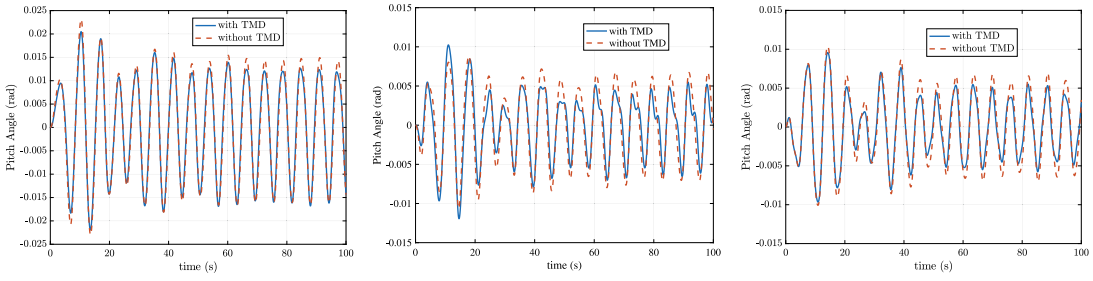

(a) Pitch angles of Component 1 (b) Pitch angles of Component 2 (c) Pitch angles of Component 3

Fig. 10. Vibration suppression results with $l = 60$ m under unified TMD parameters.

the floating foundation's vibrations. The performance indexes (which are equivalent to the averaged vibration reduction rates in this case) for $l = 120$ m, 100 m, 80 m, and 60 m are 33.02%, 47.35%, 32.49%, and 21.30%, respectively.

Then we consider using a unified set of TMD parameters to adapt to all wavelengths. To this end, we employ the following reward, which takes into account the overall performance of TMDs under different wavelengths:

$$R(x) = \sum_{j=1}^{4} h_j F_j(x) \tag{23}$$

where the index j is employed to denote different wavelengths, the constant h_j is employed for weighting purposes, and F_j follows the definition in Eq. (22). Here we set $h_1 = 0.3$, $h_2 = 0.3$, $h_3 = 0.3$, and $h_4 = 0.1$. We make such selections because the amplitudes of

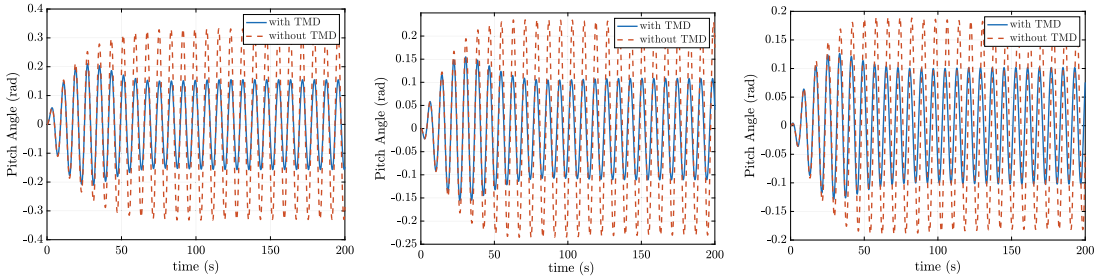

(a) Pitch angles of Component 1 (b) Pitch angles of Component 2 (c) Pitch angles of Component 3

Fig. 11. Vibration suppression results with the wave height to be 2 m and the wave direction to be 15°.

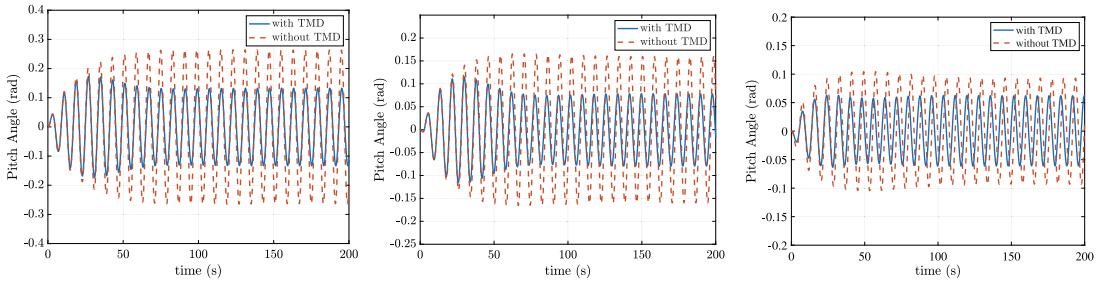

(a) Pitch angles of Component 1 (b) Pitch angles of Component 2 (c) Pitch angles of Component 3

Fig. 12. Vibration suppression results with the wave height to be 2 m and the wave direction to be 30°.

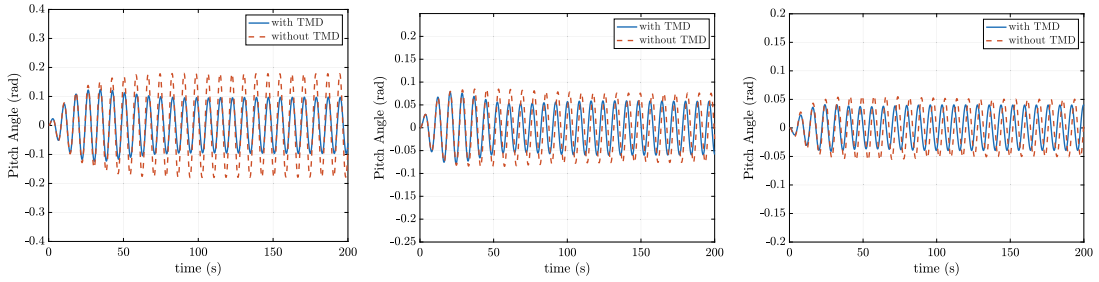

(a) Pitch angles of Component 1 (b) Pitch angles of Component 2 (c) Pitch angles of Component 3

Fig. 13. Vibration suppression results with the wave height to be 2 m and the wave direction to be 45°.

Table 1
Simulation result summary.

Case	Wavelength	$F(x^*)$	x^*
1	120 m	33.02%	$[2.52, 1.60, 1.41, 6.90, 3.14, 2.18]^{\mathrm{T}}$
2	100 m	47.35%	$[2.78, 2.00, 0.71, 1.20, 0.69, 5.52]^{\mathrm{T}}$
3	80 m	32.49%	$[0.53, 2.56, 6.03, 2.49, 6.44, 9.74]^{\mathrm{T}}$
4	60 m	21.30%	$[1.02, 3.14, 0.60, 9.57, 7.03, 2.15]^{\mathrm{T}}$

vibrations under $l = 120$ m, 100 m and 80 m are much larger than that under $l = 60$ m in our case study. Therefore, larger weighting constants (i.e., h_1, h_2 and h_3) are set for them to pursue better overall vibration suppression performance. Please notice that h_1 to h_4 are user-defined constants and they can be changed under different situations.

With the reward $R(x)$ in Eq. (23), the optimal TMD parameter setting by BA is $\boldsymbol{x}^* = [0.58, 2.38, 9.72, 2.16, 7.13, 6.45]$, and the corresponding vibration/motion suppression performance with it is illustrated in Figs. 7–10. One can see that, the passive TMDs with unified optimal parameters can successfully adapt to different wavelengths and achieve clear vibration/motion reduction for the multi-component floating structure.

It is noteworthy that wavelength is the essential environmental condition that induces structural vibrations and influences the performance of TMDs. The simulation results above show that our method is effective under different wavelengths. In addition to that, we also test the effectiveness and advantage of our TMD-based vibration suppression approach under other environmental conditions, including wave directions and heights. Particularly, we set the wavelength and height to be 100 m and 2 m, respectively, and vary the wind direction to be 15°, 30°, and 45°, respectively. Following the parameter learning result given before, the normalized TMD parameters are set to be $[2.78, 2.00, 0.71, 1.20, 0.69, 5.52]^{\mathrm{T}}$. Simulation results are given in Figs. 11–13. One can see that our method still successfully suppresses the whole floating structure's vibration under different wave heights and directions, showing its strong robustness and adaptability.

5. Conclusion

A multiple-passive-TMD structure was designed in this paper to mitigate the vibration of multi-component floating foundations. A numerical model was developed incorporating both the dynamics of a hinged floating foundation and passive TMDs. Built upon the Bayesian Ascent approach, a data-driven parameter optimization method was developed

to search for optimal TMD parameters. This sequential searching strategy combined the merits of both the Bayesian Optimization method and the gradient-free trust-region algorithm, rendering an enhanced learning efficiency. Simulation results under different wave lengths, heights and directions showed that the BA-based parameter selection method could provide optimal settings for passive TMDs, and the proposed TMD-based suppression method could significantly reduce the vibration of the multi-component floating foundation. Extended studies that may cover the wave nonlinearity & irregularity and consider different forms of physical connections between floating components will be investigated in the future to further explore the effectiveness of TMD-based approaches in vibration/motion suppression of multi-component floating structures.

CRediT authorship contribution statement

Xiantao Zhang: Conceptualization, Methodology, Investigation, Software, Formal analysis, Visualization, Writing – original draft. **Da Lu:** Conceptualization, Methodology, Investigation, Software, Data curation, Formal analysis. **Hongyang Dong:** Conceptualization, Methodology, Investigation, Software, Formal analysis, Data curation, Visualization, Writing – original draft. **Xiaowei Zhao:** Conceptualization, Methodology, Investigation, Formal analysis, Writing – review & editing, Supervision, Funding acquisition. **Feargal Brennan:** Conceptualization, Methodology, Supervision, Funding acquisition. **Yibo Liang:** Conceptualization, Methodology.

Declaration of competing interest

The authors declare that they have no known competing financial interests or personal relationships that could have appeared to influence the work reported in this paper.

Acknowledgment

This work has received funding from the UK Engineering and Physical Sciences Research Council (grant number: EP/S000747/1).

Appendix

As stated in Section 3, only heave, roll and pitch motions are considered for the floating structure. For the mathematical modeling of the hinge connector, a stiffness matrix is introduced to represent the relationship between the force of the connector and the difference of displacement at two sides of the connector, i.e.

$$\mathbf{K}_J = \begin{bmatrix} K1_1 & 0 & 0 & 0 & 0 & 0 \\ 0 & K1_2 & 0 & 0 & 0 & 0 \\ 0 & 0 & K1_3 & 0 & 0 & 0 \\ 0 & 0 & 0 & K2_1 & 0 & 0 \\ 0 & 0 & 0 & 0 & K2_2 & 0 \\ 0 & 0 & 0 & 0 & 0 & K2_3 \end{bmatrix} \tag{24}$$

where Ki_j $(i = 1, 2)$ with $j = 1, 2, 3$ represents the stiffness of the hinge connector corresponding to heave, roll and pitch motion, respectively. It is noted that for the hinge connection, two adjacent components can rotate freely around y axis whereas absolutely restricted in other degrees of freedom, indicating that the value of $Ki_3(i = 1, 2) = 0$ and $Ki_j(i = 1, 2; j = 1, 2)$ should be given a rather large value.

Since the equations of motion are established at centers of gravity of each component of the floating structure, the difference of displacement at two sides of each connector is derived based on a transformation matrix, i.e.

$$\boldsymbol{\Psi} = \begin{bmatrix} 1 & 0 & -\frac{L}{2} & -1 & 0 & -\frac{L}{2} & 0 & 0 & 0 \\ 0 & 1 & 0 & 0 & -1 & 0 & 0 & 0 & 0 \\ 0 & 0 & 0 & 0 & 0 & 0 & 0 & 0 & 0 \\ 0 & 0 & 0 & 1 & 0 & -\frac{L}{2} & -1 & 0 & -\frac{L}{2} \\ 0 & 0 & 0 & 0 & 1 & 0 & 0 & -1 & 0 \\ 0 & 0 & 0 & 0 & 0 & 0 & 0 & 0 & 0 \end{bmatrix} \tag{25}$$

All three components of the hinged floating structure have the same dimension. For a given component, the hydrostatic stiffness matrix (considering heave, roll and pitch) is calculated as follows,

$$\mathbf{C}_0 = \begin{bmatrix} \rho g A_w & 0 & 0 \\ 0 & \rho g V_w R_T & 0 \\ 0 & 0 & \rho g V_w R_L \end{bmatrix} \tag{26}$$

where ρ is the density of water, g is the gravitational acceleration, A_w is the waterplane area of each component, V_w is the displaced water volume, R_T and R_L are the transverse and longitudinal metacentric height, respectively. The hydrostatic restoring force $\mathbf{F}_h$ is then calculated as,

$$\mathbf{F}_h = \mathbf{C}\boldsymbol{\xi} = \begin{bmatrix} \mathbf{C}_0 & \mathbf{0} & \mathbf{0} \\ \mathbf{0} & \mathbf{C}_0 & \mathbf{0} \\ \mathbf{0} & \mathbf{0} & \mathbf{C}_0 \end{bmatrix} \begin{bmatrix} {}^1\boldsymbol{\xi} \\ {}^2\boldsymbol{\xi} \\ {}^3\boldsymbol{\xi} \end{bmatrix} \tag{27}$$

References

Alexander, N.A., Schilder, F., 2009. Exploring the performance of a nonlinear tuned mass damper. J. Sound Vib. 319 (1–2), 445–462.

Brochu, E., Cora, V.M., De Freitas, N., 2010. A tutorial on Bayesian optimization of expensive cost functions, with application to active user modeling and hierarchical reinforcement learning. arXiv preprint arXiv:1012.2599.

Faltinsen, O., 1993. Sea Loads on Ships and Offshore Structures, Vol. 1. Cambridge University Press.

Fitzgerald, B., Sarkar, S., Staino, A., 2018. Improved reliability of wind turbine towers with active tuned mass dampers (ATMDs). J. Sound Vib. 419, 103–122.

Hoang, N., Fujino, Y., Warnitchai, P., 2008. Optimal tuned mass damper for seismic applications and practical design formulas. Eng. Struct. 30 (3), 707–715.

Jin, C., Chung, W.C., Kwon, D.-S., Kim, M., 2021. Optimization of tuned mass damper for seismic control of submerged floating tunnel. Eng. Struct. 241, 112460.

Kundu, P., 2012. Vibration Control of Frame Structure Using Multiple Tuned Mass Dampers (Ph.D. thesis).

Lackner, M.A., Rotea, M.A., 2011. Passive structural control of offshore wind turbines. Wind Energy 14 (3), 373–388.

Li, X., Gao, H., 2015. Load mitigation for a floating wind turbine via generalized H_∞ structural control. IEEE Trans. Ind. Electron. 63 (1), 332–342.

Ou, J., Long, X., Li, Q., Xiao, Y., 2007. Vibration control of steel jacket offshore platform structures with damping isolation systems. Eng. Struct. 29 (7), 1525–1538.

Park, S., Lackner, M.A., Pourazarm, P., Rodríguez Tsouroukdissian, A., Cross-Whiter, J., 2019. An investigation on the impacts of passive and semiactive structural control on a fixed bottom and a floating offshore wind turbine. Wind Energy 22 (11), 1451–1471.

Park, J., Law, K.H., 2016. BayesIan ascent: A data-driven optimization scheme for real-time control with application to wind farm power maximization. IEEE Trans. Control Syst. Technol. 24 (5), 1655–1668.

Patil, K., Jangid, R., 2005. Passive control of offshore jacket platforms. Ocean Eng. 32 (16), 1933–1949.

Rios, L.M., Sahinidis, N.V., 2013. Derivative-free optimization: a review of algorithms and comparison of software implementations. J. Global Optim. 56 (3), 1247–1293.

Stewart, G., Lackner, M., 2013. Offshore wind turbine load reduction employing optimal passive tuned mass damping systems. IEEE Trans. Control Syst. Technol. 21 (4), 1090–1104.

Wen, B., Dong, X., Tian, X., Peng, Z., Zhang, W., Wei, K., 2018. The power performance of an offshore floating wind turbine in platform pitching motion. Energy 154, 508–521.

Wu, Z., Li, Y., 2020. Platform stabilization and load reduction of floating offshore wind turbines with tension-leg platform using dynamic vibration absorbers. Wind Energy 23 (3), 711–730.

Xu, K., Bi, K., Han, Q., Li, X., Du, X., 2019. Using tuned mass damper inerter to mitigate vortex-induced vibration of long-span bridges: Analytical study. Eng. Struct. 182, 101–111.

Yang, J., He, E., 2020. Coupled modeling and structural vibration control for floating offshore wind turbine. Renew. Energy 157, 678–694.

Yang, J., He, E., Hu, Y., 2019. Dynamic modeling and vibration suppression for an offshore wind turbine with a tuned mass damper in floating platform. Appl. Ocean Res. 83, 21–29.

Yin, X., Song, G., Liu, Y., 2019. Vibration suppression of wind/traffic/bridge coupled system using multiple pounding tuned mass dampers (MPTMD). Sensors 19 (5), 1133.

Yu, H.-F., Zhang, Y.-L., Zheng, S.-M., 2016. Numerical study on the performance of a wave energy converter with three hinged bodies. Renew. Energy 99, 1276–1286.

Zhang, B.-L., Han, Q.-L., Zhang, X.-M., 2017. Recent advances in vibration control of offshore platforms. Nonlinear Dynam. 89 (2), 755–771.

Zhang, X., Lu, D., Gao, Y., Chen, L., 2018. A time domain discrete-module-beam-bending-based hydroelasticity method for the transient response of very large floating structures under unsteady external loads. Ocean Eng. 164, 332–349.

Zhang, X., Lu, D., Liang, Y., Brennan, F., 2021. Feasibility of very large floating structure as offshore wind foundation: effects of hinge numbers on wave loads and induced responses. J. Waterw. Port Coast. Ocean Eng. 147 (3), 04021002.

Zhang, H., Xu, D., Ding, R., Zhao, H., Lu, Y., Wu, Y., 2019a. Embedded power take-off in hinged modularized floating platform for wave energy harvesting and pitch motion suppression. Renew. Energy 138, 1176–1188.

Zhang, J., Zhao, X., Wei, X., 2020. Reinforcement learning-based structural control of floating wind turbines. IEEE Trans. Syst. Man Cybern.: Syst..

Zhang, X., Zheng, S., Lu, D., Tian, X., 2019b. Numerical investigation of the dynamic response and power capture performance of a VLFS with a wave energy conversion unit. Eng. Struct. 195, 62–83.

Zhou, K., Zhang, J.-W., Li, Q.-S., 2022. Control performance of active tuned mass damper for mitigating wind-induced vibrations of a 600-m-tall skyscraper. J. Build. Eng. 45, 103646.